Effects and Optimization of Processing Parameters in Water-Assisted Injection Molding

Han-Xiong Huang, Zhi-Wu Deng

Center for Polymer Processing Equipment and Intellectualization, College of Industrial Equipment and Control Engineering, South China University of Technology, Guangzhou, People's Republic of China

Received 1 February 2007; accepted 4 October 2007
DOI 10.1002/app.27560
Published online 27 December 2007 in Wiley InterScience (www.interscience.wiley.com).

ABSTRACT: Experiments of water-assisted injection molded polypropylene curved pipe were carried out on newly developed equipment in this lab. First, four processing parameters, including short-shot size, melt temperature, water injection delay time, and water pressure, were investigated in terms of their effects on the water penetration length and residual wall thickness of curved pipe. Second, an orthogonal array of Taguchi, the *S/N* ratio, and ANOVA were utilized to find the optimal processing parameters resulting in maximum water penetration length. Finally, the crystallization behavior difference between the beginning and the end of the water channel of the curved pipe was analyzed using differential scanning calorimetry. It was interesting to find that the crystallinity of sample from the middle is higher than those from both outer and inner layers at position near the water inlet. The samples taken from the outer layer, middle, and inner layer show similar melting peak and crystallinity at position near the end of water channel. © 2007 Wiley Periodicals, Inc. J Appl Polym Sci 108: 228–235, 2008

Key words: crystallization; differential scanning calorimetry (DSC); injection molding; poly(propylene) (PP)

INTRODUCTION

Over a period of recent years, fluid-assisted injection molding technologies, including gas-assisted[1–6] and water-assisted[7–18] injection molding, have attracted more and more attention in researches and applications, due to that they offer potential to the production of complex, highly integrated parts in virtually one process step. Water- and gas-assisted injection molding (WAIM and GAIM) are similar processes and they both utilize high-pressure fluids with viscosities much lower than the polymer melt viscosity to displace the polymer melt within thick sections of the cavity. Just before demolding, the fluid is released from the core to provide a hollow but fully formed geometry. The GAIM is a well-known technology for producing hollow parts like media ducts, handles or clutch pedals. The advantages of the WAIM have made this technology an interesting alternative to the GAIM over the last few years.

In WAIM, water is used as the actuating medium. The main benefit of using water instead of gas is the much better cooling ability of water. The considerably more efficient cooling effect and high heat capacity of water result in a very efficient double sided cooling of the parts. Since the water is in direct contact with the molten polymer, cooling from the inside is even better than cooling from the outside by metal. A reduction in cycle times of about 50–70% was achieved with WAIM, when similar plastics and part geometries were compared. This potential cycle time reduction shows the productivity improvement possibilities. Moreover, WAIM has been reported to form a thinner residual wall thickness than standard GAIM and to form channels around changes in direction that are more concentric than standard GAIM; the greater inertia of the water is thought to contribute to this effect.[18] The incompressibility, low cost, and ease of recycling the water makes it an ideal medium for the process. So WAIM opens new possibilities for new and exciting applications. For example, automotive manufacturers have the potential for a broad range of cost savings with the production of fluid media piping and car door handles.

Despite the advantages associated with the WAIM process, the molding window and process control are more critical and difficult since additional processing parameters are involved. These new water-related processing parameters include the amount of melt injection, water pressure, water temperature,

Correspondence to: H.-X. Huang (mmhuang@scut.edu.cn).
Contract grant sponsor: the Guangdong Provincial Natural Science Foundation; contract grant number: 06025643.
Contract grant sponsor: Major Project of Guangzhou City; contract grant number: 2006Z2-D9081.
Contract grant sponsor: the Scientific Research Foundation for the Returned Overseas Chinese Scholars, State Education Ministry.

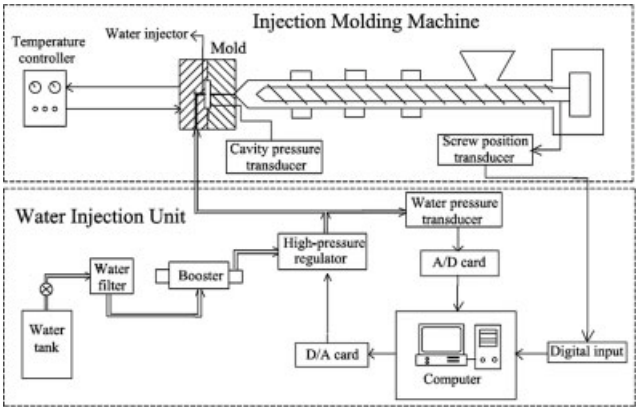

Figure 1 Schematic of experimental setup for water-assisted injection molding.

and water injection delay time.[13] Since this technique is relatively new and still in its infancy, in-depth research on the product design, machine design, mold design, the control of process parameters, and the quality of the product has not yet been conducted. Certain processing parameters in WAIM play an important role in achieving a high quality hollow part. Moreover, to the best knowledge of the authors, no research paper has ever reported the crystallization behavior of water-assisted injection molded part.

For the above-mentioned reasons, in this work, four processing variables were investigated in terms of their effects on the water penetration length and residual wall thickness in water-assisted injection molded polypropylene (PP) curved pipe. Then Taguchi method was employed to optimize the processing parameters to maximize the penetration length. Finally, the samples, taken from two positions, near the beginning and the end of the water channel, respectively, were used to analyze the crystallization behavior of molded part.

EXPERIMENTAL

Experimental set-up and material

A water injection unit, which mainly consists of a high pressure water forming and conveying unit (including its temperature controlling), a water injector, and a control circuit, was recently developed in this laboratory. The water injector used was an orifice-type. WAIM experimental investigations were carried out using the newly developed water injection unit combining with an 80-ton conventional injection molding machine, which has a highest injection rate of 84 cm^3/s. Figure 1 schematically shows the experimental setup for water-assisted injection molding. The mold used for experiments is schematically shown in Figure 2. The mold cavity is a curved one with a circular crosssection of ϕ 18 mm. The curved mold cavity has an unwound length of 387.5 mm. The temperature of the mold could be regulated by a water-circulating mold temperature controller.

In this work, a short-shot process was used, in which the mold cavity is firstly partially filled with the polymer melt followed by injecting water into the core of the polymer melt through the water injector. The water penetrates into the core of the melt and pushes the melt again to the mold wall. Finally, the polymer cools down and solidifies and a hollow product is obtained.

An injection molding grade PP, grade CJS700 from Petrochina Guangzhou Petrochemical, was used in this work. Its melt flow index is about 8.35 g/10 min (at 230°C and 2.16 kg).

Experimental methodology

The present experiments were composed of two stages: a preliminary experiment and an orthogonal experiment. First, four processing parameters, including short-shot size, melt temperature, water injection delay time, and water pressure, were selected and a preliminary experiment was conducted by changing one of the parameters in each experiment. In doing so, it was possible to better understand the effect of every processing parameter

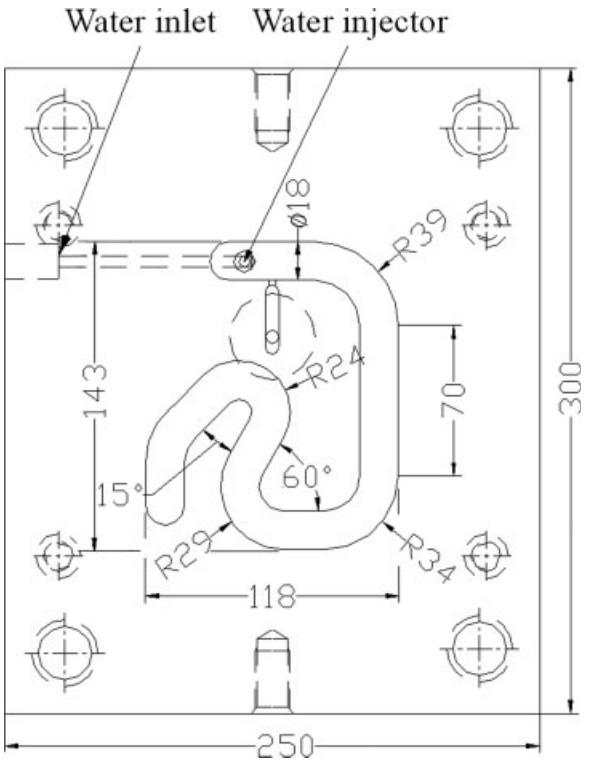

Figure 2 Schematic of mold used for water-assisted injection molding. All dimensions are in mm.

TABLE I
Processing Parameters Used in Preliminary Experiments

Processing parameters	Short-shot size (%)	Melt temp (°C)	Water pressure (MPa)	Delay time (s)
1	68.5	190	**6**	**3**
2	**73.2**	200	7	4
3	77.6	210	8	5
4	–	220	9	6
5	–	230	10	7
6	–	**240**	11	8

on the water penetration length and residual wall thickness of the water-assisted injection molded curved pipe. Moreover, the ranges of processing parameters could be determined by conducting a few experiments. Table I lists the values of these processing parameters. Preliminary experiment was performed by changing one parameter at a time and keeping the others constant (highlighted in Table I). That is, when changing one parameter in each experiment, the values highlighted were used for other processing conditions.

Second, using the same four factors as those in the preliminary experiment, an orthogonal experiment was conducted to determine the best set of processing condition that maximizes the water penetration length. Three levels for each factor were chosen using Taguchi method as shown in Table II. So nine experimental runs based on the orthogonal array L_9 (3^4) as shown in Table III were conducted. The signal-to-noise (*S/N*) ratio was used to measure the quality characteristic deviating from the desired value in Taguchi method. The water penetration lengths obtained in experiments were then analyzed to calculate the *S/N* ratio to optimize the water penetration. The maximization of the *S/N* ratio leads to the minimization of any property that is sensitive to noise. A larger water penetration length is normally required in most industry cases because that the longer the water penetrates, the more the water pressure can pack the polymer melt against the mold wall. By maximizing the water penetration length, the shrinkage as well as the sink mark at the far end of molded parts can be minimized. Therefore, the

TABLE II
Factors and their Levels in Orthogonal Experiment

Factors	Level 1	Level 2	Level 3
A: Short-shot size (%)	68.5	73.2	77.6
B: Melt temperature (°C)	210	220	230
C: Water pressure (MPa)	7	9	11
D: Water injection delay time (s)	1	3	5

TABLE III
L_9 (3^4) Orthogonal Array Used in Experiment

Exp. no.	A	B	C	D
1	1	1	1	1
2	1	2	2	2
3	1	3	3	3
4	2	1	2	3
5	2	2	3	1
6	2	3	1	2
7	3	1	3	2
8	3	2	1	3
9	3	3	2	1

larger-the-better characteristic of *S/N* ratio η was employed for the optimization of penetration length:

$$\eta = -10 \log_{10}\left(\frac{1}{n}\sum_{i=1}^{n}\frac{1}{y_i^2}\right) \quad (1)$$

where n is the number of experiments and y_i is the measured property (water penetration length in this work) for the ith experiment.

Then the response table and figure of the *S/N* ratio were obtained, from which the significant factors could be identified. The combination of each factor at the level that produces the highest *S/N* ratio would be the optimum processing condition. Using this optimum set of factors could give the maximum penetration length value in this design of experiment.

To further examine the relative significance of the processing parameters on the water penetration length, a standard analysis of variance (ANOVA) was performed.

During experiments, the control circuit in the water injection unit received a signal from the injection molding machine and controlled the time and pressure of the injected water. Five parts were molded for each set of processing conditions.

Characterizations of molded parts

The length of water penetration in molded curved pipe was measured. The residual wall thickness was measured using a digital vernier caliper with a minimum indication of 0.01 mm. The thickness measurement was conducted at five positions, P1, P3, P5, P7, and P9, as shown in Figure 3, where the number in parentheses following the position symbol represents the unwound length of corresponding position. These five positions are located at the middle of five straight zones, S1, S3, S5, S7, and S9, respectively. The measured wall thickness is a mean value, which was obtained by averaging the maximum and minimum thicknesses on the crosssection of measured position.

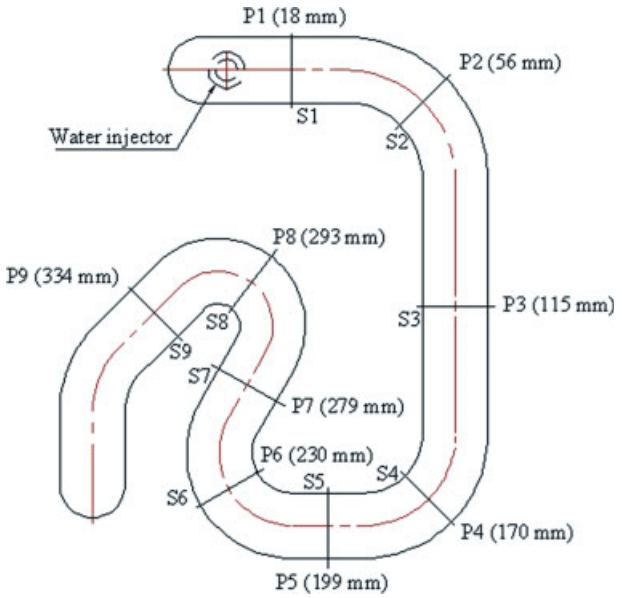

Figure 3 Schematic of molded curved pipe and positions for measuring the wall thickness. All dimensions are in mm. [Color figure can be viewed in the online issue, which is available at www.interscience.wiley.com.]

Differential scanning calorimetry (DSC) (NETZSCH DSC 204) was used to investigate the crystallization behavior of the samples taken from the part molded at 68.5% short-shot size, 230°C melt temperature, 8 s water injection delay time, and 6 MPa water pressure. Two positions, P1 and P9 as shown in Figure 3, that is, near the beginning and the end of the water channel, respectively, were chosen. Three samples, from the outer layer, middle, and the inner layer across the residual wall, respectively, were taken for each position. The slices were cut parallel to the axial direction. The DSC scans were performed in a nitrogen environment. The samples were heated from room temperature (25°C) to 200°C at a heating rate of 10°C/min.

The crystallinity of the sample can be calculated by the following equation:

$$a_c = \frac{\Delta H_m}{\Delta H_f} \times 100\% \quad (2)$$

where ΔH_m is the enthalpy used to melt sample, and ΔH_f is the heat of fusion for PP crystalline phase, which is chosen as 209 J/g referring to Ref. 19.

RESULTS AND DISCUSSION

Effects of processing parameters on penetration length and residual wall thickness of molded parts

The water penetration length in molded curved pipe was measured. Figure 4 presents the effects of four processing parameters investigated on the water

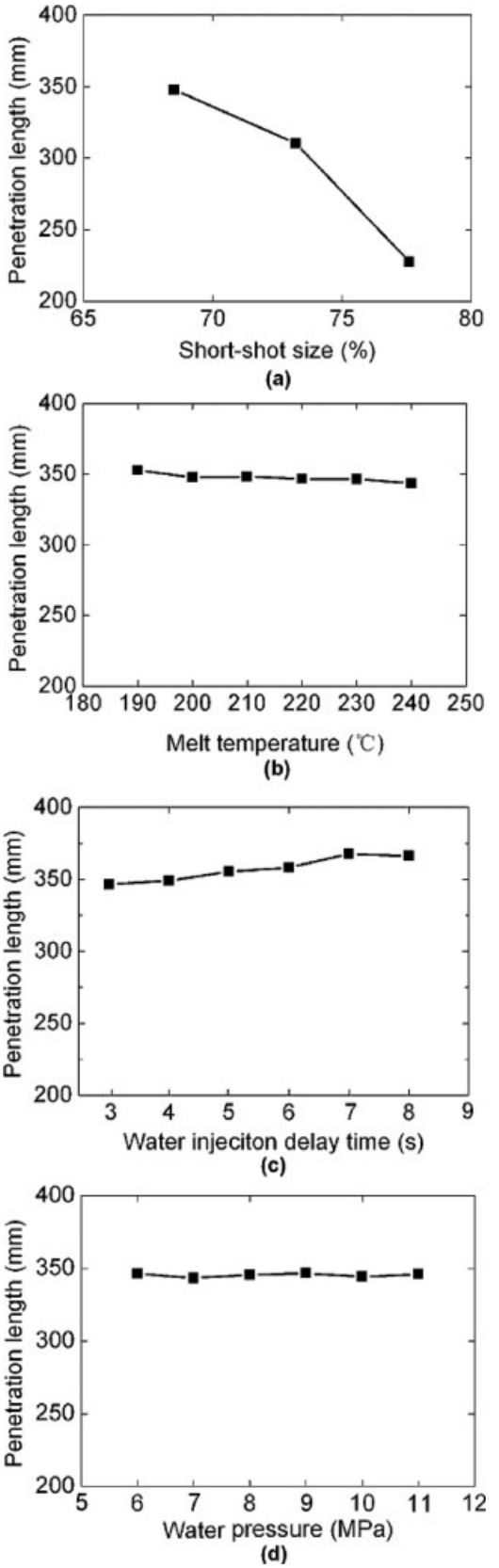

Figure 4 Effects of (a) short-shot size, (b) melt temperature, (c) water injection delay time, and (d) water pressure on water penetration length.

penetration length in molded parts. As expected, the penetration length obviously decreases with increasing the short-shot size, as shown in Figure 4(a). This is caused by the space for water being reduced as the short-shot size increases. In addition, as can be obviously seen, increasing the melt temperature slightly decreases the penetration length [as shown in Fig. 4(b)]. This may be due to that higher melt temperature decreases the thickness of the outer solidified layer of the melt and so correspondingly increases the crosssection at the beginning of the water channel. As shown in Figure 4(c), the water penetration length slightly increases with increasing the water injection delay time. This is due to the fact that increasing the delay time lengthens the cooling time and increases the thickness of the solidified layer of the melt accordingly, which decreases the crosssection at the beginning of the water channel and helps the water penetrate further into the melt core. The water pressure has little effect on the water penetration length, as shown in Figure 4(d). This may be explained as follows. There exist two phenomena in terms of its influence on the water penetration: one is that increasing the water pressure helps the water to overcome the high viscosity of the polymer melt and penetrate into the melt core; the other is that higher pressure may make the water pack the water channel and increase its void area and correspondingly increase the crosssection at the beginning of the water channel. These two contradictory phenomena have competing effects on the water penetration.

The effects of four processing parameters on the residual wall thickness in molded parts are illustrated by the thicknesses measured at five positions (P1, P3, P5, P7, and P9, as shown in Fig. 3) in Figure 5. On the whole, the residual wall thickness at position P5 is smaller than those at positions P1 and P3. Furthermore, the thickness obviously decreases from positions P7 to P9. Position P9, that is, the position near the end of the water channel, exhibits the minimum wall thickness. This can be explained as follows. At 68.5% short-shot size used in this work, the injected polymer melt can only reach near position P7 in the mold cavity. The cavity downstream is filled with the melt pushed by the water. The cavity warms up because of the contact with the hot melt during the water injection delay. While the time for the pushed melt to contact the cavity is short due to high filling rate of water. This leads the pushed melt to keep warm. Moreover, the pressure of the injected water builds up gradually due to resistance from the melt. So the water easily pushes the melt against the mold cavity.

In terms of the effects of various processing parameters on the residual thickness, it can be seen from Figure 5(a) that the short-shot size does not

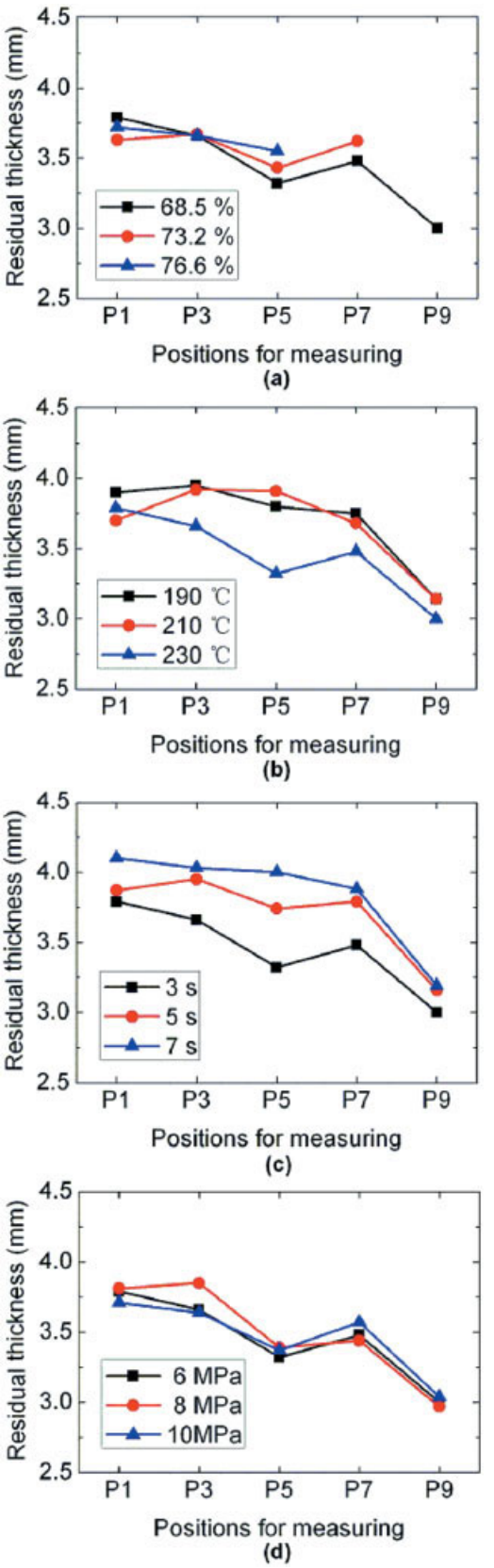

Figure 5 Effects of (a) short-shot size, (b) melt temperature, (c) water injection delay time, and (d) water pressure on residual wall thickness. [Color figure can be viewed in the online issue, which is available at www.interscience. wiley.com.]

have a notable impact on the wall thickness in the investigated range. Two contradictory phenomena occurring when increasing the short-shot size may cause this result: one is that the space for water decreases, which results in the increase of thickness; the other is that the flow resistance for water increases, which makes the water push the melt against the cavity and results in the decrease of thickness accordingly. Moreover, at 73.2 and 77.6% short-shot sizes, the water penetration lengths are 310.49 and 227.45 mm [as shown in Fig. 4(a)], respectively. So the residual thicknesses at position P9 and positions P7 and P9 can not be availably measured at 73.2 and 77.6% short-shot sizes, respectively. Increasing the melt temperature leads to the reduction of the solidified layer thickness of the melt and the corresponding decrease in residual wall thickness, as shown in Figure 5(b). From Figure 5(c) it is interesting to see that the residual thickness exhibits a clearer increment between positions P1 and P7 while only a little increase between positions P7 and P9 when increasing the water injection delay time. This is because that as previously mentioned, increasing the delay time increases the solidified layer thickness of the injected melt, the flow front of which is near position P7. This means that the thickness between positions P1 and P7 increase accordingly. As previously mentioned, the cavity beyond position P7 is filled with the melt pushed by the water. So the delay time has a little influence on the residual wall thickness between positions P7 and P9. As shown in Figure 5(d), the water pressure does not have an obvious effect on the wall thickness.

Optimization of processing parameters for maximizing penetration length of molded parts

According to the design of experiments using Taguchi method, nine trials of experiments were taken as shown in Table III. The measured water penetration lengths of molded parts were used to calculate the *S/N* ratios for the orthogonal experiment and the results are listed in Table IV. By taking the data in Table IV, the average *S/N* ratio for each level of the four factors can be obtained and the results are listed in Table V. A larger range shown in Table V indicates that the factor is more significant in affecting water penetration length.

TABLE IV
Water Penetration Lengths of Molded Parts

Exp. no.	Measured penetration length (mm)					*S/N* (dB)
	y_1	y_2	y_3	y_4	y_5	
1	319.58	330.33	330.90	322.63	334.38	50.30
2	355.09	353.21	353.72	355.47	346.01	50.94
3	346.17	352.94	335.86	331.34	336.98	50.63
4	308.47	295.23	294.71	295.43	299.78	49.50
5	275.33	280.40	280.88	274.29	278.05	48.87
6	287.97	289.02	290.33	287.72	292.90	49.23
7	239.16	237.10	234.18	234.84	230.68	47.42
8	242.47	243.34	244.14	244.14	241.02	47.71
9	227.42	219.95	220.47	224.99	221.66	46.95

TABLE V
Average *S/N* Ratios by Factor Levels (dB)

Factors	A	B	C	D
Level 1	50.62	49.07	49.08	48.71
Level 2	49.20	49.17	49.13	49.20
Level 3	47.36	48.94	48.97	49.28
Range	3.26	0.23	0.16	0.57

From Table V, it can be observed that among the four factors investigated, the most significant factor that affecting the water penetration length is the short-shot size, whereas the melt temperature, water pressure, and water injection delay time are not significant factors. The optimum set of factors can be determined from the *S/N* ratio response by selecting the level with the highest *S/N* value of each factor. The result is a combination of A1, B2, C2, and D3 as the best set of factors. These optimized factor levels corresponds to a short-shot size of 68.5%, a melt temperature of 220°C, a water pressure of 9 MPa, and a water injection delay time of 5 s.

The combination of above-obtained optimum factor levels is not included in the main experiment shown in Table III, so the *S/N* response value of the water penetration length corresponding to the optimized factor levels was predicted as follow:

$$\eta_{A1B2C2D3} = \eta_m + (\eta_{A1} - \eta_m) + (\eta_{B2} - \eta_m) + (\eta_{C2} - \eta_m) + (\eta_{D3} - \eta_m) \quad (3)$$

where η_m is the mean *S/N* ratio for the nine experiments in the orthogonal experiment and η_{Fj} is the *S/N* ratio for factor *F* and level *j*. Using eq. (3), the predicted *S/N* ratio of the water penetration length for the optimized factor levels, A1/B2/C2/D3, is 44.04 dB. This predicted value is indeed higher than those obtained in the orthogonal experiment (Table IV). This implies that the above-obtained optimum factor levels can properly increase the water penetration length in molded parts.

A confirmation experiment was conducted by utilizing the levels of optimized factor levels. The measured average length of water penetration in molded parts was 355.99 mm. So, the penetration length is increased compared with those attained in the orthogonal experiment, as shown in Table IV.

The data in Table IV were further analyzed by using an ANOVA technique. The degree of freedom, sum of square, and percentage contribution were calculated and the results are shown in Table VI. From Table VI, it is apparent that factor A has the most

TABLE VI
ANOVA for Penetration Length of Molded Parts

Factors	Degree of freedom	Sum of square	Percentage contribution (%)
A	2	16.06	95.85
B	2	0.08	0.49
C	2	0.04	0.22
D	2	0.58	3.44
Total	8	16.76	100.00

significant contribution, which is 95.85%, so it is a significant affecting parameter for maximum penetration length. Whereas factors B, C, and D have much less contribution, so they are not a significant affecting parameter.

Crystallization behavior of molded parts

Shown in Figure 6 are the DSC curves of the slices cut from the outer layer, middle, and inner layer across the residual wall of curved pipe. The correspondent heating enthalpy, melting peak temperatures, and crystallinity are listed in Table VII. As can be directly observed, the DSC melting peak of samples from the middle and inner layer is slightly higher than that from the outer layer for position P1. The sample from the inner layer exhibits an obviously sharp peak shape. It is interesting to see that the crystallinity of sample from the middle is higher than those from both outer and inner layers. The sample from the inner layer exhibits the lowest crystallinity (31.8%). This can be explained by the heat

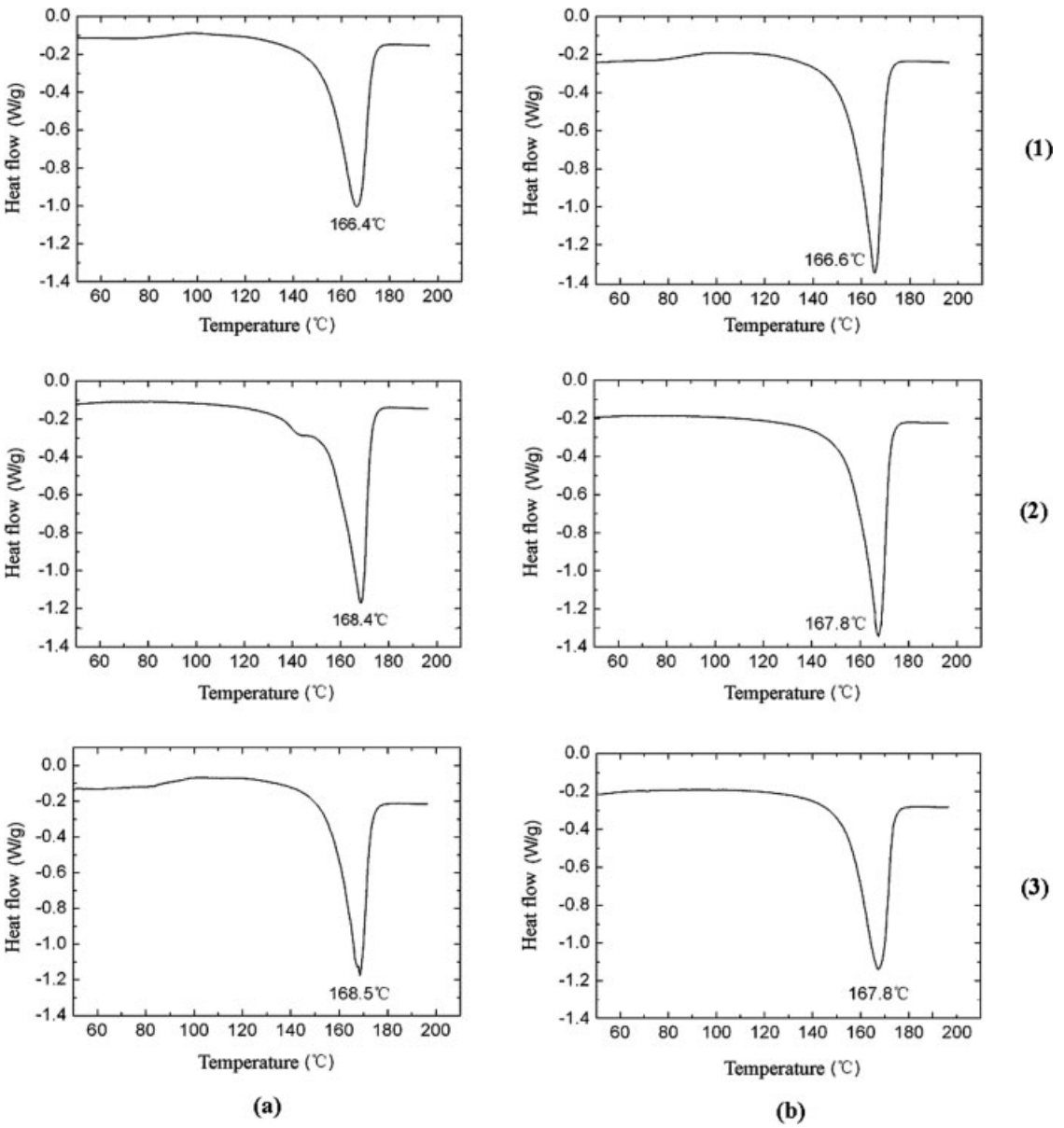

Figure 6 DSC curves for samples from (1) outer layer, (2) middle, and (3) inner layer at positions (a) 1 and (b) 9.

TABLE VII
Melting Enthalpy ΔH_m, Melting Peak Temperature T_m, and Crystallinity a_c for Samples Across the Wall of Molded Part

Samples	ΔH_m (J/g)	T_m (°C)	a_c (%)
P1			
Outer	77.36	166.4	37.0
Middle	88.84	168.4	42.5
Inner	66.42	168.5	31.8
P9			
Outer	81.96	166.6	39.2
Middle	84.17	167.8	40.3
Inner	81.96	167.8	39.9

transfer occurring in the WAIM process as follows. At position P1, the melt layer contacting with the cold mold cavity cools down quickly. Moreover, during the initiation of water injection, the water temperature at position P1 is the lowest since it is near the water inlet. The inner melt layer (in contact with the water) cools faster than the outer layer (in contact with the mold), due to the higher heat capacity of the water. Quick temperature reduction in turn results in relatively lower crystallinity, especially for the sample taken from the inner layer. Meanwhile, the melt at the middle across the thickness cools down slowly due to low thermal conductivity of polymer. This means that the melt at the middle takes a longer time to cool, which in turn leads to relatively higher crystallinity.

At position P9, the samples taken from the outer layer, middle, and inner layer show similar melting peak and crystallinity. This may be attributed to the fact that the mold cavity corresponding to this position is filled up by melt pushed under the water. The mold cavity warms up because of the contact with the hot melt during the water injection delay (8 s) and the water also warms up when reaching position P9 because of the heat absorbed from hot melt during its penetration. Moreover, position P9 exhibits obviously thinner residual wall than position P1, as shown in Figure 5. So the cooling rate difference across the wall is not so obvious as that at position P1. It is reasonable to deduce that the crystallinity of samples taken from other different locations across the wall of position P9 is also similar.

Comparing the results of positions P1 and P9, it can be seen that for the inner layer, position P9 exhibits higher crystallinity than position P1. For the outer layer, the former shows relatively higher crystallinity; whereas for the middle, the latter exhibits relatively higher crystallinity. The reason is the same as that mentioned above.

CONCLUSIONS

A water injection unit was developed in this laboratory, which was used with a conventional injection molding machine to investigate the influence of short-shot size, melt temperature, water injection delay time, and water pressure on the water penetration length and residual wall thickness of water-assisted injection molded curved PP pipe. By using Taguchi method, nine trials were run. The optimum parameters that can maximize the penetration length are: short-shot size (68.5%), melt temperature (220°C), water pressure (9 MPa), and water injection delay time (5 s). Among these four factors, the short-shot size is the most effective factor, whereas the melt temperature, water injection delay time, and water pressure are not significant factors. It was found from DSC results that the crystallinity of sample from the middle is higher than those from both outer and inner layers at position near the water inlet. The samples taken from the outer layer, middle, and inner layer show similar melting peak and crystallinity at position near the end of water channel.

References

1. Avery, J. Gas-Assist Injection Molding—Principles and Applications; Hanser Gardner Publications: Munich, 2001.
2. Turng, L. S. Adv Polym Technol 1995, 14, 1.
3. Zhou, H. M.; Li, D. Q. J Appl Polym Sci 2003, 90, 2377.
4. Chien, R. D.; Chen, S. C.; Lin, M. C.; Lee, P. H.; Chen, C. S. J Appl Polym Sci 2003, 90, 2979.
5. Polynkin, A.; Pittman, J. F. T.; Sienz, J. Polym Eng Sci 2005, 45, 1049.
6. Smith, G. F.; Magalhaes, R. Plast Rubber Compos 2005, 34, 247.
7. Michaeli, W.; Brunswick, A.; Gruber, M. Kunstst Plast Eur 1999, 89, 20.
8. Michaeli, W.; Brunswick, A.; Pohl, T. Kunstst Plast Eur 1999, 89, 18.
9. Michaeli, W.; Brunswick, A.; Kujat, C. Kunstst Plast Eur 2000, 90, 25.
10. Michaeli, W.; Brunswick, A.; Pfannschmidt, O. Kunstst Plast Eur 2002, 92, 38.
11. Jüntgen, T.; Michaeli, W. SPE ANTEC Tech Pap 2002, 386.
12. Knights, M. Plast Technol 2002, 48(4), 42.
13. Liu, S. J.; Chen, Y. S. Polym Eng Sci 2003, 43, 1806.
14. Protte, R.; Bangert, H.; Cooper, C.; Hoeck, P. SPE ANTEC Tech Pap 2003, 404.
15. Liu, S. J.; Chen, Y. S. Compos A 2004, 35, 171.
16. Chang, R. Y.; Huang, C. T.; Yang, W. H.; Tsai, M. H.; Lu, K. I.; Liu, S. J. SPE ANTEC Tech Pap 2004, 566.
17. Lang, S.; Parkinson, M. J. Plast Rubber Compos 2005, 34, 232.
18. Liu, S. J.; Lin, S. P. Adv Polym Technol 2006, 25, 9.
19. Rachtanapun, P.; Selke, S. E. M.; Matuana, L. M. J Appl Polym Sci 2003, 88, 2842.